Journal of Luminescence 236 (2021) 118058

Contents lists available at ScienceDirect

Journal of Luminescence

journal homepage: http://www.elsevier.com/locate/jlumin

OSL response of α-Al_2O_3:C, Mg exposed to beta and UVC radiation: A comparative investigation

J.M. Munoz [a], L.S. Lima [b], E.M. Yoshimura [b], L.G. Jacobsohn [c], N.M. Trindade [a,b,*]

[a] Department of Physics, Federal Institute of Education, Science and Technology of São Paulo, São Paulo, SP, Brazil
[b] Institute of Physics, University of São Paulo - USP, São Paulo, SP, Brazil
[c] Department of Materials Science and Engineering, Clemson University, Clemson, SC, USA

ARTICLE INFO

Keywords:
Al_2O_3:C,Mg
UVC irradiation
Beta irradiation
OSL
Color centers

ABSTRACT

Continuous wave optically stimulated luminescence (CW-OSL) of an Al_2O_3:C, Mg single crystal was investigated after irradiation with ultraviolet C radiation (UVC; peak emission at 254 nm) as well as with a beta source under different doses (100 mGy – 3 Gy). Analysis of the OSL decay curves provided experimental evidence that: i) UVC- and beta-irradiated Al_2O_3:C, Mg single crystal showed similar OSL decay curves, and that ii) a same fast ($\tau \sim 2.9$ s) and a same slow ($\tau \sim 29$ s) components were identified in the OSL decay curves for both types of radiation. On the other hand, analysis of the results suggested that radiation type generated distinct initial concentration of charges trapped at these two traps. The differences in the OSL decay curves were attributed either to differences in the initial population of the traps or to a balance of trapping-detrapping during UV irradiation.

1. Introduction

Although ultraviolet radiation (UV) in the UVC range (100–280 nm) emitted by the sun does not reach Earth's surface because it is completely absorbed by stratospheric O_2 and O_3 [1], artificial UVC lamps are widely used. Applications include sterilization of food and food packaging, disinfection of surgical materials and tools, water treatment, and extermination of airborne microorganisms in operating rooms [2,3]. In general, mercury discharge lamps used for these applications are referred to as "germicidal lamps", "bactericidal lamps" or simply "UVC lamps" [2]. Besides the usefulness of UVC radiation, UV overexposure, and UVC in particular, can lead to severe health problems such as erythema, cataract formation, skin cancer and selective immune deficiency [2,4]. Health surveillance and safety practices regarding exposure to UV are in place for occupational exposed individuals [5]. On the other hand, UV radiation can contribute to the luminescence emission of dosimetric materials. Within this context, we investigated the influence of the UVC radiation in the optically stimulated luminescence (OSL) response of an Al_2O_3:C, Mg single crystal.

The OSL technique is based on the release of charges from traps in the band gap followed by radiative recombination at a luminescence center and thus is similar to thermoluminescence (TL). However, instead of elevated temperatures like in TL, in the OSL case detrapping is stimulated by the absorption of light [6]. OSL emission arises from the recombination of charges optically released from traps in a material previously exposed to ionizing radiation, and its intensity can be related to the absorbed irradiation dose [6–8]. The OSL signal obtained under stimulation with constant light power (continuous wave OSL; CW-OSL) is observed as a decay curve, *i.e.*, it progressively decreases in time since the total amount of charges trapped is finite in number [7,9]. The function that models CW-OSL considering j recombination centers (RC) and i traps is shown in Equation (1):

$$I_{cw}(t) = \sum_{j}^{RC} \sum_{i}^{traps} \rho_{RCj}\rho_{RRj}\ \eta_j C_i\ p_i\ exp(-p_i t) = \\ = \left[\sum_{j}^{RC} \rho_{RCj}\rho_{RRj}\ \eta_j \right] \cdot \left[\sum_{i}^{traps} C_i\ p_i\ exp(-p_i t) \right] \quad (1)$$

where $I_{cw}(t)$ is the total detected OSL emission corresponding to the summation of the OSL emission from all combinations of i traps and j recombination centers. In Eq. (1), ρ_{RCj} corresponds to the probability of electron-hole recombination at RC_j, ρ_{RRj} to the probability of radiative recombination (RR) of RC_j, η_j to the quantum efficiency of the detector at the emission wavelength of RC_j, C_i to constants that include the initial population of trap i and geometrical factors involving light collection and transport towards the detector, p_i is the probability rate of a trapped

* Corresponding author. Department of Physics, Federal Institute of Education, Science and Technology of São Paulo, São Paulo, SP, Brazil.
E-mail address: ntrindade@ifsp.edu.br (N.M. Trindade).

https://doi.org/10.1016/j.jlumin.2021.118058
Received 10 August 2020; Received in revised form 10 March 2021; Accepted 13 March 2021
Available online 19 March 2021

electron to transition to the conduction band from a trap i where $p_i = \phi\sigma_i$, with σ_i being the photoionization cross section of trap i related to the optical stimulation wavelength and ϕ the light stimulation intensity, t is the stimulation time, and τ_i is the time constant of OSL such that $p_i = \frac{1}{\tau_i}$ [7,10,11]. Eq. (1) assumes no retrapping, no interaction between the traps, no interaction between the recombination centers, and no saturation effects. It means that for each trap i recombination can occur at j possible recombination centers, each with its own probability of radiative recombination ρ_{RRj}, and that the fate of an electron released in the conduction band does not affect the fate of the next released electron. Since $\sum_{j}^{RC} \rho_{RCj}\rho_{RRj}\ \eta_j = \alpha$, where α is a constant, Eq. (1) can be simplified such that the first summation becomes a multiplying factor to the second summation:

$$I_{cw}(t) = \alpha \sum_{i}^{traps} C_i\ p_i\ exp(-p_i t) \tag{2}$$

Al_2O_3:C, Mg was introduced by Akselrod et al. [12] in the early 2000's. It is a bright luminescent material because the carbon and magnesium co-doping of the Al_2O_3 host promotes the formation of single vacancy defects like F, F(Mg), F^+ and F^+(Mg) color centers. In addition to them, a variety of aggregate color centers such as F_2, F_2^+, F_2^{2+}, F_2^+(Mg), F_2^+(2 Mg) and F_2^{2+}(2 Mg) have also been observed [13–15]. Furthermore, this material has been shown to be an efficient radiation sensor when exposed to X-rays [16], beta rays [14,16,17], gamma rays [18], neutrons, protons and other charged particles [19]. The OSL and TL investigation of this material showed a direct relationship between both phenomena: illuminating a beta-irradiated single crystal with blue light reduced the TL signal, and heating the beta-irradiated material eliminated the OSL signal [20].

Recently, our group investigated the TL response of UV-irradiated Al_2O_3:C, Mg [21]. The TL results showed three low-intensity peaks at about 320 K (peak I), 350 K (peak II) and 375 K (peak III), while the main peak (peak IV) was at 455 K (heating rate of 1 K/s). Comparison between UV and beta irradiations showed similar glow curves. On the other hand, a linear response with the beta irradiation dose was observed, whereas UV irradiation led to a saturating exponential TL response as a function of the radiation exposure. In this work, we further this investigation to the OSL response of Al_2O_3:C, Mg to UVC irradiation.

2. Materials and methods

An Al_2O_3:C, Mg single crystal grown by the Czochralski method [12,22] provided by Landauer, Inc., Crystal Growth Division, Stillwater, OK, USA, was used. The single crystal had 48 mg and a rectangular parallelepiped shape 8 × 1.6 × 0.5 mm^3.

UVC irradiation was executed with different nominal energy densities, from 4.78 × 10^2 to 1.43 × 10^4 J/m^2, with the sample placed 30 cm directly below the lamp. The UV irradiation system was composed by a Boitton lamp model BOIT-LUB01, with two 6 W UV-emitting bulbs, one in the UVA (315–400 nm main emission at 365 nm (3.40 eV)) and the other in the UVC (nominal irradiance 4.78 mW/cm^2, emission at 254 nm (4.88 eV)) regions of the spectrum. Only the results obtained with the UVC bulb are presented, as the sample did not show any sensitivity to UVA irradiations up to 60 s. Given the typical emission spectra of Hg lamps in the UVC range, within the context of this work UVC radiation was considered electromagnetic radiation with wavelength 254 nm. For comparison purposes, beta irradiation was executed using the built-in $^{90}Sr/^{90}Y$ source of the TL/OSL Risø reader delivering a dose rate of 10 mGy/s and cumulative doses from 0.1 to 3 Gy.

OSL measurements were carried out at room temperature (RT) using an automated Risø TL/OSL reader, model DA-20, DTU Nutech. The OSL signal was stimulated in CW mode using blue LEDs (470 nm (2.64 eV), FWHM = 20 nm (2.58–2.70 eV), 80 mW/cm^2 at the sample position). Thermal treatment (inside the Risø reader, from RT to 300 °C at 5°C/s followed by natural cooling down to RT) was carried out after each OSL readout without exposing the sample to any source of light to make sure traps were empty before a new irradiation was executed. In addition, after each OSL readout, an optical stimulation was performed with the same blue LED for 60 s, to completely bleach the OSL signal. These values were also used to subtract the background of the signal from each response. As such, a delay of about 1 min Occurred between any irradiation and the OSL readout. The OSL signal was detected by a bialkali photomultiplier tube Hamamatsu H7421-40 behind a 1 mm dia. collimator and a UV-transmitting visible-absorbing filter (Hoya U-340, 7.5 mm thickness) to block the stimulation light while transmitting the UV part (*ca.* 260–390 nm (3.18–4.77 eV)) of the OSL signal. Exponential fittings of the OSL decay curves were done based on equation (2). In our analysis of approximately 20 decay curves total either UVC- or beta-irradiated, only two components ($i = 1, 2$) were found necessary to obtain a good fitting ($R^2 > 0.99$, where R^2 is the coefficient of determination).

Monte Carlo simulations of the electron irradiation of Al_2O_3 were performed; composition and physical parameters closest to Al_2O_3:C,Mg, available in the database of the ESTAR program [23] were used. The simulations were executed using the PENEPOLE (Penetration and Energy Loss of Positrons and Electrons)/penEASY computer code version 2019 [24]. For the calculation, a detailed description of the $^{90}Sr/^{90}Y$ beta source was included, describing the energy spectrum and source dimensions (0.05 cm thick and radius of 0.5 cm, aluminum cap), and the materials between the source and sample (0.1 cm thick aluminum attenuator, 0.0125 mm thick quartz window and 7.3 mm thick layer of air between the source and the sample). The geometry and mass of the Al_2O_3:C, Mg sample were also reproduced in the calculations.

The radioactive source was simulated using the PENNUC package [25], with the radioactive files (Y-90. nuc for example) obtained from the Laboratoire National Henri Becquerel (LNHB). Results presented in this work correspond to the average of the calculations of forty-million individual electrons. The transport parameters C_1 and C_2 that control the cutoff for elastic collisions were both chosen as 0.1 keV; WCC and WCR, which are the cutoffs for inelastic and bremsstrahlung interactions, were set as, respectively, 100 keV and 10 keV; the cutoff for absorption energy was fixed as 10 keV for charged particles and photons.

3. Results and discussion

Fig. 1 illustrates a comparison of the normalized OSL decay curves

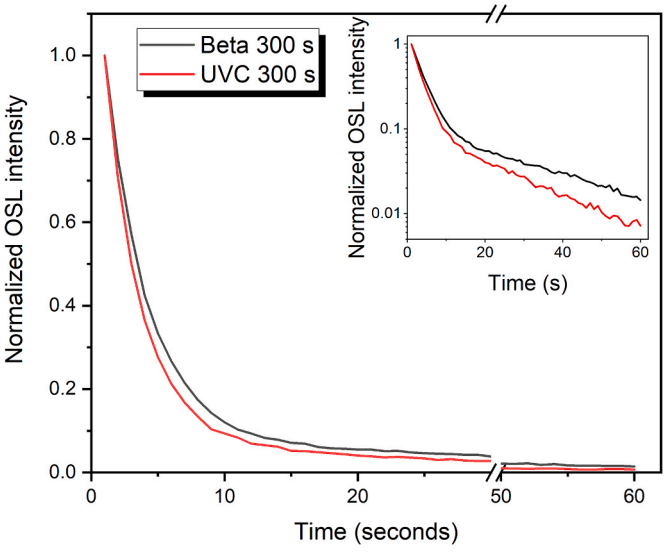

Fig. 1. Normalized OSL curves after 300 s UVC (red line) and beta (black line) irradiations. The inset shows the same results in a semi-log plot.

obtained after beta (black line) and UVC (red line) irradiation for 300 s. This comparison showed that the curve shapes depended on the type of radiation used. The curves were similar at the beginning but as the stimulation time increased, the OSL decay of the UVC-irradiated sample became faster than that for the beta-irradiated one. The differences between the decay curves are highlighted in the inset where a semi-log plot of the same results is presented.

In order to understand the blue-stimulated OSL signal of the sample irradiated by different types of radiation, it is important to consider the specific conditions in which these measurements were executed and how the energy of each type of radiation was absorbed and dissipated in Al_2O_3:C, Mg. The OSL process involves at least one type of trap and at least one type of recombination center. In Al_2O_3:C, Mg, a variety of recombination centers have been reported [14] and they are summarized in Table 1. Considerably less is known about the traps, though F-type centers are thought to be electron traps [26].

When beta radiation is used to irradiate the Al_2O_3:C, Mg single crystal, numerous electron-hole pairs are created in the whole volume, while direct ionization of the color centers is unlikely. Some electron-hole pairs promptly recombine radiatively (radioluminescence) or non-radiatively, while the remaining electrons and holes migrate through the material possibly being captured by traps or other defects, including color centers. At least the capture of holes by F centers has already been reported in sapphire under 1.8 MeV electron irradiation [29]. Measurements of the emission spectrum of green (540 nm; 2.30 eV) stimulated OSL readout of beta-irradiated Al_2O_3:C, Mg showed F and F^+ centers to be the only recombination centers [30].

In the case of UVC (in this work, essentially 4.88 eV), a variety of phenomena occurs. Defect-free Al_2O_3 is essentially transparent to 4.88 eV radiation [31], and it is the presence of color centers with absorption bands in this spectral region that creates strong absorption of this radiation. F^+(Mg), F^+, and F_2^+(2 Mg) color centers absorb around 4.86, 4.8, and 4.77 eV (Table 1), respectively, thus, 4.88 eV irradiation generates photoluminescence from these color centers. Indeed, photoluminescence at about 1.9 and 3.7 eV was reported from Al_2O_3:C, Mg under 4.8 and 4.9 eV irradiation, respectively [14]. On the other hand, at least the photoionization of F^+(Mg) centers by 4.77 eV (260 nm) light, and of F_2^+(2 Mg) centers by 3.82 eV (325 nm) light [27] has already been reported. Consequently, irradiation with higher energy light, as performed here (4.88 eV), is expected to be able to ionize all but F and F(Mg) centers. Particularly, F_2, F_2^+(Mg), F_2^+(2 Mg), and F_2^{2+}(2 Mg) that have absorption energies within 2.0 and 4.1 eV (Table 1) are ionized. Ultimately, because of the specific energy of the UVC irradiation, all but F and F(Mg) color centers became the source of free electrons that eventually populate all traps within the band gap as well as holes that are trapped at the ionized color centers.

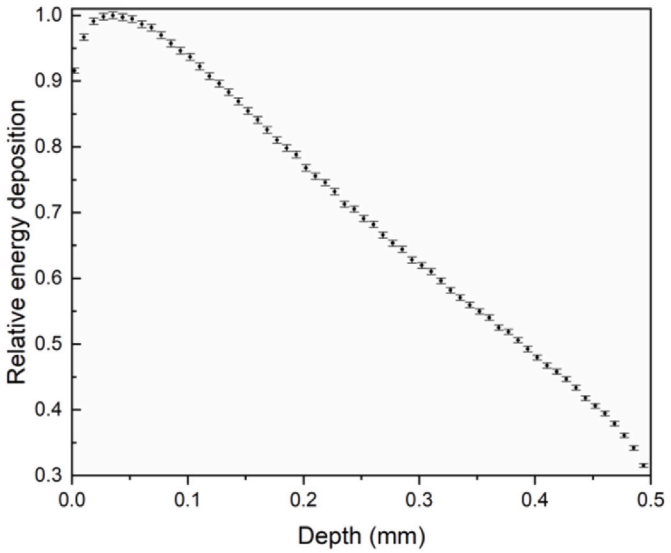

Fig. 2. Results of Monte Carlo simulation of the relative energy deposition in the Al_2O_3:C, Mg sample irradiated by the built-in beta source of the Risø reader.

It is also important to consider the spatial distribution of electron-hole pairs created by the two types of radiation. In the case of beta radiation, the Monte Carlo simulation gives rise to the results seen in Fig. 2 that shows the relative energy deposition per gram in the sample, along its depth. For various depths in the sample, it was checked that the energy deposition is very homogeneous along a plane parallel to the sample surface (results not shown here). These results indicate that the whole sample receives energy from the beta source, and that the creation of electron-hole pairs is distributed throughout the whole sample. In the case of UVC irradiation, color centers were assumed to be homogeneously distributed throughout the sample. UVC radiation absorption and thus photoionization of color centers is expected to follow Beer-Lambert's law, *i.e.*, corresponds to a decreasing exponential from the surface into the sample. Based on absorption measurements reported earlier [14], the absorption coefficient of F centers at 204 nm, F^+ centers at 255 nm and F_2^{2+}(2 Mg) centers at 435 nm was estimated to be 35 cm^{-1}, 1.9 cm^{-1} and 1.0 cm^{-1}, respectively. The attenuation lengths of 0.282 mm for 204 nm radiation and 5.36 mm for 255 nm radiation due to F and F^+ centers, respectively, show that 204 nm radiation is fully absorbed by about half of the thickness of the crystal, while 255 nm irradiates the full thickness of the crystal. Thus, some UVC radiation irradiates the whole crystal, although with decreasing intensity along the depth. On the other hand, all other F-type centers could be affected

Table 1
Absorption and emission energies of color centers in α-Al_2O_3:C, Mg according to Refs. [26–28]. The expected major effect of 254 nm (4.88 eV) irradiation on the color centers is displayed on column 3. The detectability by the Risø reader based on the optical transmission of the Hoya U-340 filter (260–390 nm; 3.18–4.77 eV) is in the last column.

Color center	Absorption (eV)	Effect of UVC irradiation (@ 254 nm; 4.88eV)	Emission (eV)	Emission detected?
F/F(Mg)	6.0	–	3.0	Partially
F^+	5.4	–	3.8	Yes
	4.8	Absorption/Photoionization		
F^+(Mg)	5.17	–	3.82	Yes
	4.86	Absorption/Photoionization		
F_2	4.1	Photoionization	2.48	No
	3.5	Photoionization		
	2.75	Photoionization		
F_2^+(Mg)	3.54	Photoionization	3.22	Yes
F_2^+(2 Mg)	4.77	Absorption/Photoionization	1.65	No
	3.7	Photoionization		
	2.0	Photoionization		
F_2^{2+}(2 Mg)	2.85	Photoionization	2.43	No

by the incoming UVC radiation throughout the whole thickness of the crystal.

In addition to irradiation, the effects of blue light stimulation (2.64 eV, FWHW = 2.58–2.70 eV) and readout conditions need to be considered as well. First of all, the major effect of blue stimulation is the release of electrons from traps as deep as ~2.70 eV during OSL measurements. The use of a Hoya U-340 filter during OSL readout allows the detection only of emissions within 3.18–4.77 eV (260–390 nm), *i.e.*, emissions from F^+, F^+(Mg), F_2^+(Mg), and partially from F/F(Mg) color centers. Actually, the fact that CW stimulation was used in these measurements implies that all available recombination centers could contribute to the luminescence being generated; however, only the emission of F^+, F^+(Mg), F_2^+(Mg), and partially from F/F(Mg) color centers could be detected due to the specific experimental conditions of this work. In practice, the OSL decay curves recorded in this work correspond to the convoluted measurement of the probability of different traps being emptied as a function of time using F^+, F^+(Mg), F_2^+(Mg), and F/F(Mg) as recombination centers. Eq. (1) could be adjusted to this experimental situation by making $\eta_j = 0$ for all recombination centers emitting out of the detectable range. This implies that the constant α in Eq. (2) corresponds to a sum of fewer terms.

In order to extract additional information, OSL decay curves were analyzed using Eq. (2). It was found that two exponential decays were needed to obtain a good fit to the experimental data, in agreement with visual analysis of the inset in Fig. 1. This result indicated that two different types of traps were participating in the OSL response of this material, *i.e.*, $i = 1, 2$. Further, the combined results of the independent fittings of all OSL curves revealed that the probability rate of trapped electrons to transition to the conduction band from traps i, p_1 and p_2, could be grouped around mean values, $\bar{p}_i$. Importantly, the same $\bar{p}_1$ and $\bar{p}_2$ mean values could be used for beta and UVC irradiations, as the distributions of p_i values corresponding to each irradiation were compatible within 3 standard deviations (99.5% confidence). Consequently, fitting with two exponential components was evaluated again, this time using the weighted mean values of the p_i probabilities, found before, as fixed parameters. The weighted mean values of the p_i probabilities were obtained using weighted least squares:

$$\bar{p}_i(i=1,2) = \sum_k \frac{p_{i_k}}{s_{i_k}^2}(k=1 \ \ to \ \ 20) \tag{3}$$

where $s_{i_k}^2$ is the squared uncertainty of p_i obtained through the fitting of the kth-OSL decay curve considering the results obtained from both radiation types for each component. These new fittings achieved high correlation coefficients ($R^2 > 0.99$) for both radiation types and all irradiation. Fig. 3 illustrates the fitting results of OSL decay curves obtained after 3 Gy irradiation with beta (Figs. 3a) and 1.43×10^4 J/m^2 of UVC (Fig. 3b). In these plots, the individual exponential components are shown as black and red continuous lines, and their sum as a continuous blue line. From this analysis, the resulting representative weighted probabilities were: $p_1 = (3.47 \pm 0.01) \times 10^{-1}$ s^{-1} and $p_2 = (3.47 \pm 0.05) \times 10^{-2}$s^{-1}.

In summary, the analysis of OSL decay curves for both types of radiation resulted in two components: a fast and a slow. The respective time constant (τ) and photo-ionization cross section (σ) values under 470 nm stimulus are: fast component ($\bar{p}_1$): $\tau_1 = (2.885 \pm 0.007)$ s and $\sigma_1 = (1.835 \pm 0.005) \times 10^{-18}$ cm^2, and slow component ($\bar{p}_2$): $\tau_2 = (28.9 \pm 0.4)$ s and $\sigma_2 = (1.83 \pm 0.02) \times 10^{-19}$ cm^2. According to Ref. [32], the CW-OSL decay curves of Al_2O_3:C exposed to beta radiation also presented two components with photoionization cross-sections $\sigma_1 = 1.51 \times 10^{-18}$ cm^2 and $\sigma_2 = 5.02 \times 10^{-19}$ cm^2. These values were of the same order of magnitude as the ones found in this work and differences were tentatively attributed to the effects of the introduction of Mg as a co-dopant in the host. Based on the results found in this work, and within the framework of Eq. (1), it was possible to conclude that differences in the OSL curves obtained from beta- and UVC-irradiated Al_2O_3:C, Mg

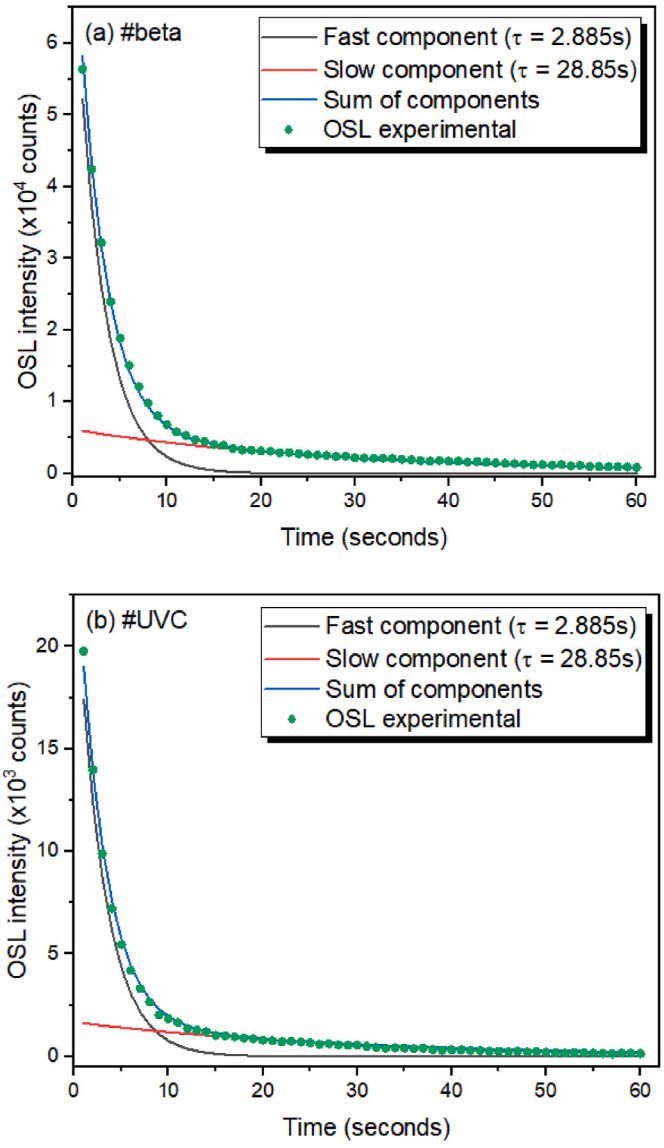

Fig. 3. OSL experimental results (green dots), as well as best fit results: fast component (black line), slow component (red line), and sum of the two components (blue line) for Al_2O_3:C, Mg single crystal exposed to (a) 3 Gy of beta radiation and (b) 1.43×10^4 J/m^2 of UVC radiation.

(Fig. 1) were due to differences in the initial populations, n_{0i} ($i = 1,2$), of the two traps involved, and that the same pair of traps was involved regardless the type of radiation used.

Fig. 4 shows the behavior of the integral of the OSL decay curve (area under the curve) as a function of the UVC energy density and beta dose. These curves are equivalent to dose-response curves, as the irradiation time is proportional to the energy delivered to the sample by UV or beta radiation sources. The behavior of the integral of the OSL curves as a function of the dose was best-fitted using a linear function for the beta irradiation, and a saturating exponential function for the UVC case [21]:

$$I(D) = a + b \times t \tag{4}$$

$$I(E) = c \times \left(1 - e^{-dt}\right). \tag{5}$$

In these equations, *I(D)* and *I(E)* is the OSL curve integral as a function of dose D and energy density E for beta and UVC exposure, respectively, b the slope, a the linear intercept (fixed at the origin in the best fit, *i.e.*, $a = 0$), c a proportionality constant, and d an exponential factor related to the irradiation time needed to reach saturation. The

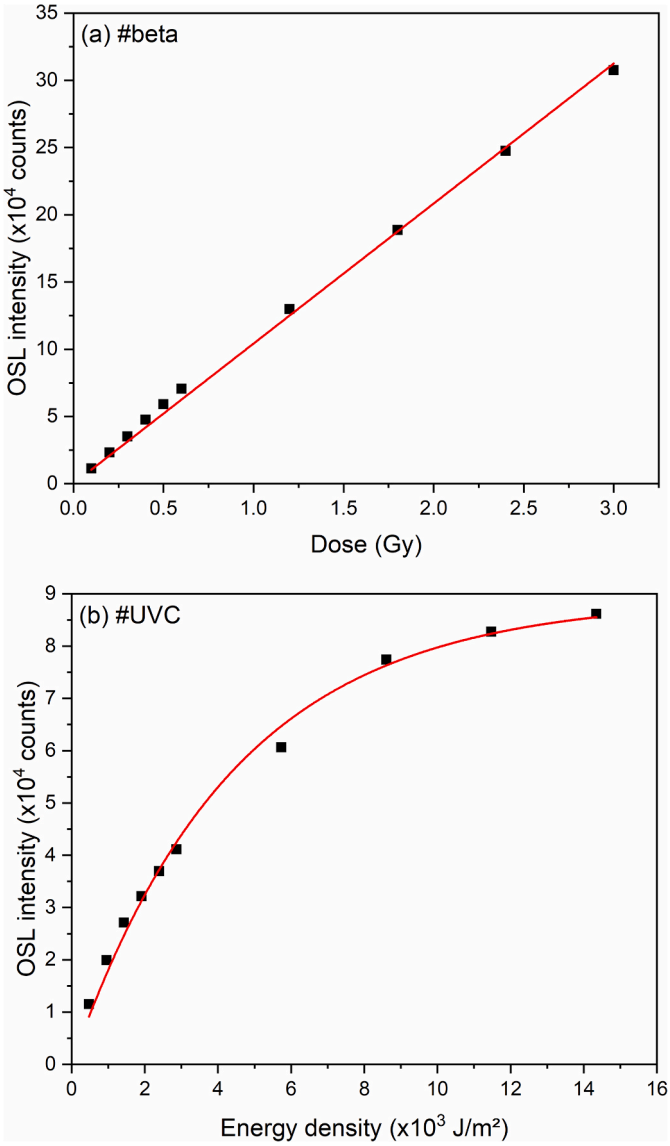

Fig. 4. Integrated intensity (area) of OSL decay curves as a function of (a) beta dose and (b) UVC energy density together with best fittings (continuous lines). See text for details.

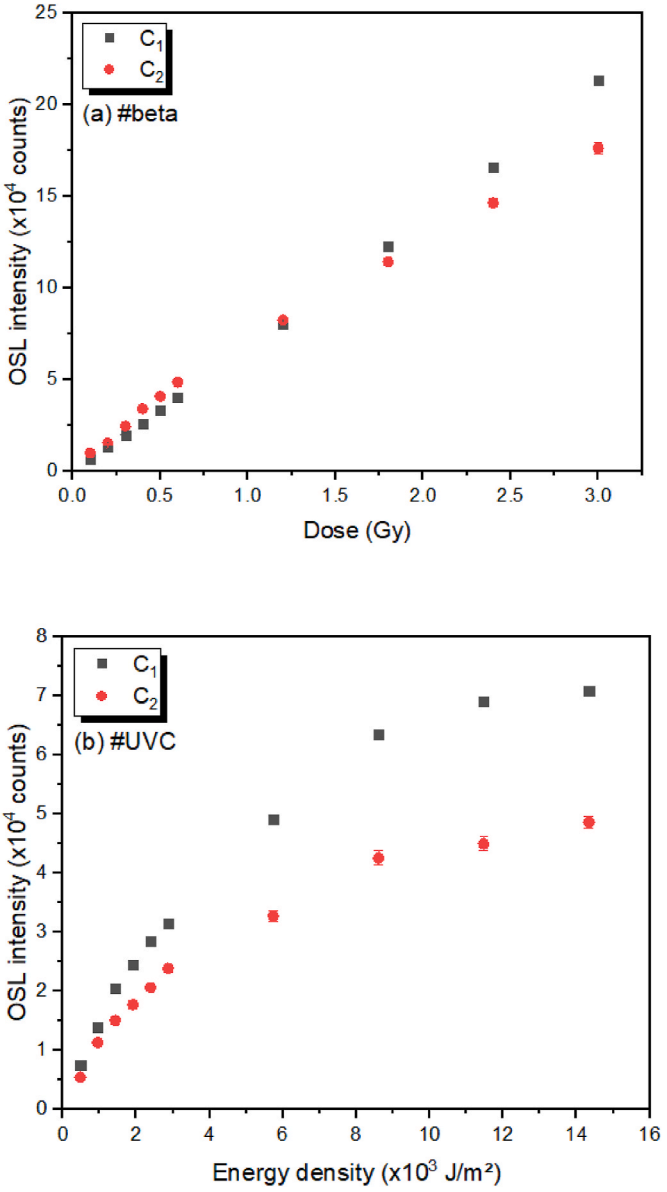

Fig. 5. C_i coefficients associated to fast ($i = 1$; black symbols) and slow ($i = 2$; red symbols) components as functions of (a) beta dose and (b) UVC energy density.

Table 2
Best fit results of the OSL integral intensity of beta- and UVC-irradiated Al_2O_3: C, Mg.

beta irradiation (Eq. (4))	UVC irradiation (Eq. (5))
$a = 0$	$c = (8.9 \pm 0.2) \times 10^5$
$b = (1.04 \pm 0.01) \times 10^3$ s^{-1}	$d = (2.7 \pm 0.1) \times 10^{-4}$ s^{-1}
$R^2 = 0.999$	$R^2 = 0.993$

resulting fitting parameters and the respective coefficient of determination, R^2, are shown in Table 2.

Nevertheless, the reason for saturation of the OSL signal after UVC irradiation remains to be explained. Fitting of the OSL experimental results to Eq. (2) allowed us to gain insight into C_i that are constants related to the initial concentration of trap i, n_{0i}, and geometrical factors involving light collection and transport towards the detector. Since the geometrical factors are fixed, the behavior of C_i is representative of the behavior of n_{0i}. The behavior of C_i as a function of dose and energy density is shown in Fig. 5a and (b) for both beta and UVC irradiations. Results for beta irradiation are shown as closed circles and for UVC irradiations as closed squares, while results related to $i = 1$ are presented in black, and to component $i = 2$ are in red.

Interestingly, for each type of radiation, the values of both C_i were within the same order of magnitude, with larger relative differences observed for longer irradiation times, especially for UVC irradiation, as discussed below. In particular, the C_1 and C_2 values for both types of radiation were remarkably similar for small irradiation doses (about 300 mGy for beta radiation and 3×10^3 J/m^2 for UVC radiation). For beta irradiation, this behavior continued up to 1.8 Gy. However, in contrast to the linear growth in time of both C_i associated to beta irradiation, saturation of both C_i associated to UVC irradiation was observed for energy deposition greater than 3×10^3 J/m^2. Moreover, the relative contribution of the slow component ($i = 2$) decreased for greater energy deposition, reaching about 40% of the total trapped charges at 1.43×10^4J/m^2). In the case of beta irradiation, some evidence of the beginning of saturation of the slow component was observed after 1.8 Gy of dose, while the fast component continued to increase linearly in time. After 3

Gy, the population related to the slow component was reduced to 83% in comparison to the population related to the fast component for beta radiation.

Saturation of the integral of an OSL decay curve for long irradiation times could be due to: i) relatively low number of electron-hole pairs released during irradiation, ii) relatively low concentration of available traps, iii) relatively low concentration of recombination centers, and iv) trapping-detrapping of charges by UV during irradiation. The fact that under beta radiation C_1 continued to grow linearly while C_2 showed signs of saturation rules out causes i) and iii), assuming that there is no correlation between the nature and the spatial distribution between the traps and the recombination centers. These results suggested saturation was due to a relatively low concentration of the traps responsible for the slow decay component of the OSL curve (assumption $i = 2$), leading to a non-linear increase behavior of n_{02} with the beta irradiation time. In the case of UVC, after 1.4×10^3 J/m^2 of energy density, both n_{0i} showed signs of saturation. A similar reasoning indicates that, for UVC irradiation, both n_{0i} have a saturating behavior. Another possibility is that UV radiation leads to a balance of trapping-detrapping (assumption iv), giving rise to weaker OSL signals with a saturation behavior. As discussed earlier, the source of electron-hole pairs for UVC irradiation were F^+, F^+(Mg), F_2, F_2^+(Mg), F_2^+(2 Mg), and F_2^{2+}(2 Mg) color centers. While F^+(Mg), F^+, and F_2^+(2 Mg) could photoluminesce under UVC irradiation, at least the photoionization of F^+(Mg) and F_2^+(2 Mg) under UV irradiation has already been reported. Because of the experimental conditions used in this work, OSL measurements were particularly sensitive to the populations of F^+, F^+(Mg), F_2^+(Mg), and to some extent also of F/F(Mg) color centers. Further, the decreasing exponential (Lambert-Beer law) that describes UVC absorption and the low kinetic energy of the free electrons generated by UVC probably limits the volume in which UVC irradiation takes effect, giving rise to a small concentration of charges in the trapping centers.

4. Conclusions

An investigation of the OSL response of Al_2O_3:C, Mg single crystal irradiated by UVC was executed considering the response to beta irradiation as a reference. While the OSL decay curves were different in shape depending on the type of radiation used, they all could be described by two decreasing exponential functions using the same pair of probability rates of trapped electrons to transition to the conduction band from traps i ($i = 1, 2$). This analysis yielded a $\tau_1 = (2.885 \pm 0.007)$ s fast component with photoionization cross-section $\sigma_1 = (1.835 \pm 0.005) \times 10^{-18}$ cm^2, and a $\tau_2 = (28.9 \pm 0.4)$ s slow component with $\sigma_2 = (1.83 \pm 0.02) \times 10^{-19}$ cm^2. These results supported an earlier observation that the main TL trap was also involved in the OSL mechanism [20]. Further, the differences in the OSL decay curves were attributed to differences in the initial population of the traps, n_{0i}, as inferred by the behavior of C_i, or to a balance of trapping-detrapping during UV irradiation. The behavior of the integral of the OSL response as a function of irradiation time showed saturation of both n_{0i} under UVC irradiation after 3×10^3 J/m^2 irradiation, and only of n_{02} after 1.8 Gy under beta irradiation. Analysis of these results considered the differences in the absorption and dissipation of the energy of the incoming radiation. In the case of UVC, saturation could be attributed to the limitation of the volume in which UVC irradiation takes effect, giving rise to a small concentration of charges in the trapping centers, or to a double action of UVC, *i.e.*, ionization of defects and also releasing charges from trapping centers populated during illumination. The OSL response of Al_2O_3:C, Mg to UVC and beta radiations was similar, such that exposure to a mixed field may not be recognizable by the shape of the OSL decay curve alone.

Author statement

J. M. Munoz: Investigation, Formal analysis, Data curation, Writing – original draft. L. S. Lima: Investigation, Formal analysis, Data curation, Writing – original draft. E. M. Yoshimura: Resources, Supervision, Writing-Review&Editing. L. G. Jacobsohn: Resources, Supervision, Writing-Review&Editing. N. M. Trindade: Conceptualization, Methodology, Validation, Writing – original draft, Writing-Review&Editing.

Declaration of competing interest

The authors declare that they have no known competing financial interests or personal relationships that could have appeared to influence the work reported in this paper.

Acknowledgments

J.M. Munoz (#2019/22375–2) and N.M. Trindade (#2019/05915–3) are grateful to São Paulo Research Foundation (FAPESP). L.G. Jacobsohn is grateful to the National Science Foundation, grant #1653016. E. M. Yoshimura is grateful to São Paulo Research Foundation (FAPESP), grant #2018/05982–0 and National Council for Scientific and Technological Development (CNPq), grant #306843/2018–8. The authors are grateful to Dr. M.S. Akselrod with Landauer, Inc., Crystal Growth Division, Stillwater, OK, USA, for providing the Al_2O_3:C, Mg single crystal. In addition, the authors are indebted to H.F. Brito, L.G. Merízio, M.G. Magalhães, M.C.S. Nunes and L. E. Caldas for their help with the methodology of the measurements.

References

[1] P. Kullavanijaya, H.W. Lim, Photoprotection, J. Am. Acad. Dermatol. 52 (2005) 937–958, https://doi.org/10.1016/j.jaad.2004.07.063.
[2] P. Vecchia, Protecting Workers from Ultraviolet Radiation, International Commission on Non-Ionizing Radiation Protection, Oberschleibheim, 2007.
[3] M. Begum, A.D. Hocking, D. Miskelly, Inactivation of food spoilage fungi by ultra violet (UVC) irradiation, Int. J. Food Microbiol. 129 (2009) 74–77, https://doi.org/10.1016/j.ijfoodmicro.2008.11.020.
[4] V.H. Oliveira, N.M. Khaidukov, E.C. Silva, L.O. Faria, Study of TL properties of $LaAlO_3$:Ce,Dy crystals for UV dosimetry, Radiat. Meas. 46 (2011) 1173–1175, https://doi.org/10.1016/j.radmeas.2011.08.022.
[5] E. Okuno, Epidemiologia do câncer devido a radiações e a elaboração de recomendações, Rev. Bras. Física Médica. 3 (2009) 43–55, https://doi.org/10.29384/RBFM.2009.V3.N1.P43-55.
[6] E.G. Yukihara, S.W.S. Mckeever, Optically Stimulated Luminescence: Fundamentals and Applications, UK: John Wiley and Sons, West Sussex, 2011.
[7] L. Botter-Jensen, S.W.S. McKeever, A.G. Wintle, Optically Stimulated Luminescence Dosimetry, Elsevier Science, Amsterdam, 2003, https://doi.org/10.1016/B978-0-444-50684-9.X5077-6.
[8] A.S. Pradhan, J.I. Lee, J.L. Kim, Recent developments of optically stimulated luminescence materials and techniques for radiation dosimetry and clinical applications, J. Med. Phys. 33 (2008) 85–99, https://doi.org/10.4103/0971-6203.42748.
[9] L. Bøtter-Jensen, Development of Optically Stimulated Luminescence Techniques Using Natural Minerals and Ceramics, and Their Application to Retrospective Dosimetry, University of Copenhagen, 2000.
[10] A. Bluszcz, G. Adamiec, Application of differential evolution to fitting OSL decay curves, Radiat. Meas. (2006), https://doi.org/10.1016/j.radmeas.2006.05.016.
[11] A.J.J. Bos, J. Wallinga, Optically stimulated luminescence signals under various stimulation modes assuming first-order kinetics, Phys. Rev. B Condens. Matter 79 (2009) 195118, https://doi.org/10.1103/PhysRevB.79.195118.
[12] M.S. Akselrod, A.E. Akselrod, S.S. Orlov, S. Sanyal, T.H. Underwood, New aluminum oxide single crystals for volumetric optical data storage, Opt. Data Storage. 13 (2003), https://doi.org/10.1364/ODS.2003.TuC3. TuC3.
[13] G.M. Akselrod, M.S. Akselrod, E.R. Benton, N. Yasuda, A novel Al_2O_3 fluorescent nuclear track detector for heavy charged particles and neutrons, Nucl. Instrum. Methods Phys. Res. Sect. B Beam Interact. Mater. Atoms 247 (2006) 295–306, https://doi.org/10.1016/j.nimb.2006.01.056.
[14] N.M. Trindade, L.G. Jacobsohn, Thermoluminescence and radioluminescence of α-Al_2O_3:C,Mg at high temperatures, J. Lumin. 204 (2018) 598–602, https://doi.org/10.1016/j.jlumin.2018.08.018.

[15] J.M. Kalita, M.L. Chithambo, On the sensitivity of thermally and optically stimulated luminescence of α-Al_2O_3:C and α-Al_2O_3:C,Mg, Radiat. Meas. 99 (2017) 18–24, https://doi.org/10.1016/j.radmeas.2017.03.006.
[16] M.G. Rodriguez, G. Denis, M.S. Akselrod, T.H. Underwood, E.G. Yukihara, Thermoluminescence, optically stimulated luminescence and radioluminescence properties of Al_2O_3:C,Mg, Radiat. Meas. 46 (2011) 1469–1473, https://doi.org/10.1016/j.radmeas.2011.04.026.
[17] J.M. Kalita, M.L. Chithambo, The effect of annealing and beta irradiation on thermoluminescence spectra of α-Al_2O_3:C,Mg, J. Lumin. 196 (2018) 195–200, https://doi.org/10.1016/j.jlumin.2017.12.036.
[18] N.S. Saharin, H. Wagiran, A.R. Tamuri, Thermoluminescence (TL) properties of Al_2O_3: C, Mg exposed to cobalt-60 gamma radiation doses, Radiat. Meas. 70 (2014) 11–14, https://doi.org/10.1016/j.radmeas.2014.08.012.
[19] M.S. Akselrod, G.J. Sykora, Fluorescent nuclear track detector technology – a new way to do passive solid state dosimetry, Radiat. Meas. 46 (2011) 1671–1679, https://doi.org/10.1016/j.radmeas.2011.06.018.
[20] N.M. Trindade, L.G. Jacobsohn, E.M. Yoshimura, Correlation between thermoluminescence and optically stimulated luminescence of α-Al_2O_3:C,Mg, J. Lumin. 206 (2019) 298–301, https://doi.org/10.1016/j.jlumin.2018.10.084.
[21] N.M. Trindade, M.G. Magalhães, M.C.S. Nunes, E.M. Yoshimura, L.G. Jacobsohn, Thermoluminescence of UV-irradiated α-Al_2O_3:C,Mg, J. Lumin. 223 (2020) 117195, https://doi.org/10.1016/j.jlumin.2020.117195.
[22] C.D. Brandle, Czochralski growth of oxides, J. Cryst. Growth 264 (2004) 593–604, https://doi.org/10.1016/j.jcrysgro.2003.12.044.
[23] M.J. Berger, J.S. Coursey, M.A. Zucker, J. Chang, ESTAR, PSTAR, and ASTAR: Computer Programs for Calculating Stopping-Power and Range Tables for Electrons, Protons, and Helium Ions, National Institute of Standards and Technology, Gaithersburg, MD, 2005, https://doi.org/10.18434/T4NC7P [Online] Available:, version 1.2.3. http://physics.nist.gov/Star. (Accessed 21 December 2020).
[24] J. Sempau, A. Badal, L. Brualla, A PENELOPE -based system for the automated Monte Carlo simulation of clinacs and voxelized geometries-application to far-from-axis fields, Med. Phys. 38 (2011) 5887–5895, https://doi.org/10.1118/1.3643029.
[25] E. García-Toraño, V. Peyres, F. Salvat, PENNUC: Monte Carlo simulation of the decay of radionuclides, Comput. Phys. Commun. 245 (2019), https://doi.org/10.1016/j.cpc.2019.08.002.
[26] B.D. Evans, G.J. Pogatshnik, Y. Chen, Optical properties of lattice defects in α-Al_2O_3, Nucl. Instrum. Methods Phys. Res. Sect. B Beam Interact. Mater. Atoms 91 (1994) 258–262, https://doi.org/10.1016/0168-583X(94)96227-8.
[27] G.J. Sykora, M.S. Akselrod, Photoluminescence study of photochromically and radiochromically transformed Al_2O_3:C,Mg crystals used for fluorescent nuclear track detectors, Radiat. Meas. 45 (2010) 631–634, https://doi.org/10.1016/j.radmeas.2009.11.022.
[28] N.M. Trindade, L.G. Jacobsohn, Thermoluminescence and radioluminescence of α-Al2O3:C,Mg at high temperatures, J. Lumin. 204 (2018) 598–602, https://doi.org/10.1016/j.jlumin.2018.08.018.
[29] A. Moroño, E.R. Hodgson, On the origin of the F+ centre radioluminescence in sapphire, J. Nucl. Mater. 249 (1997) 128–132, https://doi.org/10.1016/S0022-3115(97)00227-4.
[30] G. Denis, M.G. Rodriguez, M.S. Akselrod, T.H. Underwood, E.G. Yukihara, Time-resolved measurements of optically stimulated luminescence of Al_2O_3:C and Al_2O_3:C,Mg, Radiat. Meas. 46 (2011) 1457–1461, https://doi.org/10.1016/j.radmeas.2011.06.054.
[31] E.W.J. Mitchell, J.D. Rigden, P.D. Townsend, The anisotropy of optical absorption induced in sapphire by neutron and electron irradiation, Philos. Mag. A J. Theor. Exp. Appl. Phys. 5 (1960) 1013–1027, https://doi.org/10.1080/14786436008235880.
[32] A. Soni, D.R. Mishra, Mathematical formulation of Tmax-Tstop method for LM-OSL and its experimental validation on α-Al_2O_3:C, Nucl. Instr. Methods Phys. Res. Sect. B Beam Interact. with Mater. Atoms. 375 (2016) 87–92, https://doi.org/10.1016/j.nimb.2016.03.039.